Journal of Materials Chemistry A

Accepted Manuscript

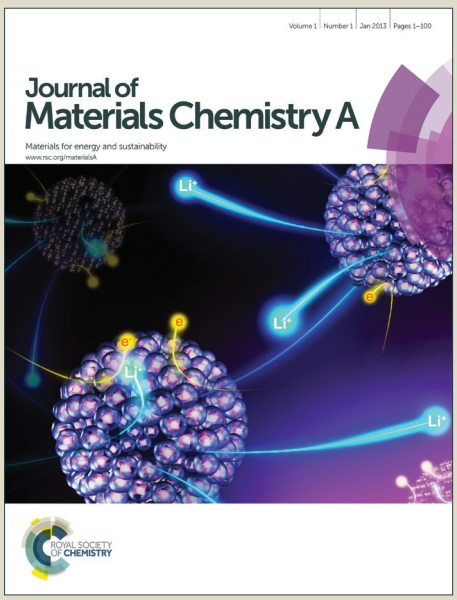

ROYAL SOCIETY OF CHEMISTRY

www.rsc.org/materialsA

Shape Effects of Pt Nanoparticles on Hydrogen Production via Pt/CdS Photocatalysts Under Visible Light

Muhua Luo[1], Weifeng YAO[1*], Cunping Huang[2], Qiang Wu[1], Qunjie Xu[1]
[1]Shanghai Key Laboratory of Materials Protection and Advanced Materials in Electric Power, College of Environmental & Chemical Engineering, Shanghai University of Electric Power, Shanghai 200090, P. R. China. [2]Aviation Research Division, FAA William J. Hughes Technical Center, Atlantic City International Airport, NJ 08405, USA

Abstract

The shape effects of Pt cocatalysts on the photocatalytic activity of Pt/CdS for hydrogen production were investigated for the first time. Nano-cubic and nano-spherical Pt particles were prepared via a shape-and-size-controlled technology and loaded onto a CdS semiconductor photocatalyst for visible light photocatalytic hydrogen production from an aqueous ammonium sulfite solution. Unlike conventional photodeposition and impregnation methods, shape-controlled synthesis is able to produce cubic Pt cocatalysts with tunable sizes. Pt nanocubes loaded Pt/CdS photocatalysts show strong shape enhanced photocatalytic activity compared to those of Pt nanospheric particle loaded Pt/CdS photocatalysts. Under the same Pt loading and Pt particle size the efficiencies of Pt nanocubes loaded Pt/CdS catalysts is 52% and 31% higher than that of Pt nanospheres loaded Pt/CdS photocatalysts at 5.7nm and 4.0nm, respectively. In comparing with Pt/CdS photocatalysts prepared via photodeposition, more than 25% efficiency improvement has been achieved with the Pt nanocubes loaded Pt/CdS photocatalyst. The electrochemical characterization of Pt nanoparticles revealed that photocatalytic activities of Pt/CdS photocatalysts rely on both the shape and size of Pt particles. The higher the electrocatalytic activity of the Pt nanoparticles, the higher the efficiency of photocatalytic hydrogen evolution.

1. Introduction

Semiconductor-metal nanocomposites have been widely employed in photocatalytic water splitting/reducing for hydrogen production. Metal particles in contact with the semiconductor considerably enhance the efficiency of photocatalysis.[1, 2] Overall, the photocatalytic water splitting/reducing process involves three major steps: Step 1: light absorption by a semiconductor based photocatalyst for the generation of electron-hole pairs; Step 2: electrons and holes separation and migration to the photocatalyst surface; and Step 3: subsequent redox reactions on the surface of photocatalyst particles (Scheme 1). Based on these three steps a number of

technologies have been developed to improve the efficiency of photocatalytic water splitting. These include (1) development of narrow band gap semiconductor materials to absorb a broader spectrum of solar radiation (Step 1); (2) materials design and preparation to increase the crystallinity of photocatalyst particles and to optimize particle size for efficient charge separation and transportation (Step 2); and (3) semiconductor band engineering to match the redox potential of water reducing and oxidation (Step 3). Principally, the major challenge of photocatalytic hydrogen production is the recombination of charges that leads to efficiency loss.

For the alleviation of charge recombination and the reduction of overpotentials necessary for hydrogen generation, noble metal particles are required to be deposited onto the surface of a photocatalyst to form semiconductor-metal nanocomposites.[1-6] In a photocatalytic process, noble metal particles play a mediating role for storing and shuttling the photo-generated electrons from the semiconductor to an electron acceptor (adsorbed H^+) (Scheme 1A). In principle, due to the difference of work functions, a Schottky barrier would be formed at their interface when a metal particle makes contact with a semiconductor.[7] The Schottky barrier can facilitate the separation of the electrons and holes and enhance the photocatalytic efficiency. When a metal with a larger work function is in contact with a semiconductor, the Fermi level of the metal is shifted to a more negative potential required by the Fermi-level equilibration.[8] Therefore, Pt noble metal with a large work function of 5.65eV is preferred as the most effective cocatalyst for trapping electrons and catalyzing proton reduction in the semiconductor-metal interface.[1, 6]

In photocatalytic water splitting, because proton reduction actually occurs on the noble metal surface (Scheme 1A), the activity of proton catalytic reduction over a noble metal particle strongly influences the efficiency of a metal/semiconductor photocatalyst. Similar to photocatalytic water splitting/reducing, the electrocatalytic water splitting/reducing also takes place on the surface of a noble metal electrode. In accordance with the photocatalytic proton reduction, the electrochemical activity of an electrode is determined by the catalytic activity of the noble metal (Scheme 1B). This similarity indicates that the photocatalytic activity of a noble metal/semiconductor photocatalyst for water splitting/reducing is related to the electrocatalytic activity of the noble metal.

It is well known that electrocatalytic activities of noble metal electrodes are sensitive to the size and shape of metal particles. Metal atoms located in corners and edges of a particle are

unsaturated active sites with different adsorption geometry and desorption energy, and are therefore more active compared to the atoms located on the surface of the particle. [9-11] The shape of noble metal particles plays an equally important role as the particle size in the reduction of activation energy of an electrochemical process. [12, 13] Inspired by the similarity between photocatalysis and electrocatalysis, this research investigates the shape effects of Pt nanoparticles on the photocatalytic activity of Pt/CdS photocatalysts. Pt metal was selected as an example because of its widespread application as cocatalyst in photocatlytic water splitting/reducing for hydrogen production.

Conventionally, nanosized metal particle loaded photocatalysts are prepared using photodeposition or impregnation techniques. [3-5, 14] However, it is almost impossible using these conventional technologies to control the shape and size of metal particles because the metal particles prepared via these methods grow on the surface of a semiconductor crystal and form only spherical particles.[1-5] A few new methods were recently developed for controlling the size of metal cocatalyst particles. For example, Berr et al. successfully prepared Pt clusters smaller than 2nm and loaded them onto a CdS surface using a laser ablation source.[15-19] Kudo et al. coated Au clusters over CdS using glutathione-protected Au_{25} clusters.[20] However, few research efforts achieved control of the shapes of metal cocatalyst particles. A facile and reproducible method to control both shapes and sizes of Pt metal cocatalysts is reported in this research as: (1) shape controlled synthesis of nanosized Pt particles using liquid phase reduction of Pt ions and (2) loading the prepared particles onto a photocatalyst surface, similar to the preparation of electrocatalysts.[4, 6, 9] This strategy may be applicable to metal cocatalysts other than the Pt nanocubes reported here.

2. Experimental methods for Pt nanoparticle preparation

2.1 Synthesis of Pt nanocubes and nanospheres: The conditions for Pt nanoparticle preparation were similar to those described previously.[21] In detail, a total of 0.05mmol of ammonium hexachloroplatinate ($(NH_4)_2Pt(IV)Cl_6$) and potassium tetrachloroplatinate ($K_2Pt(II)Cl_4$) was dissolved in 10mL of ethylene glycol in a 25mL three-necked round-bottom flask at room temperature. Tetramethylammonium bromide (0.75mmol) and polyvinylpyrrolidone (PVP) (K30, 111mg) were added to the solution under magnetic stirring. The mixture was heated to 180°C (which is lower than the 197.3°C of ethylene glycol boiling temperature) under argon for 20min.

The product was then collected by centrifugation and washed using ethanol and cyclohexane to remove ethylene glycol and partially remove the PVP capping agent. The complete removal of PVP was carried out using a facile $NaBH_4$/tert-butylamine (TBA) combined treatment technology.[22] The obtained Pt particles were then re-dispersed in ethanol for further use. The size of cubic Pt particles was controlled by the molar ratios of Pt(IV)/(Pt(II) + Pt(IV)). Pt nanocubes with average sizes of 8nm, 6nm and 4nm were synthesized at the molar ratios of 100%, 80% and 20%, respectively. (The sizes in this research refer to the average edge lengths of nanocubes). Pt nanospherical particles with average diameters of 4.0nm and 5.7nm were prepared based on 20% and 80% molar ratios of Pt(IV)/(Pt(II) + Pt(IV)), respectively. The heating temperature was controlled at 140°C and the other experimental conditions were identical to those in the synthesis of cubic Pt particles.

2.2 Preparation of Pt(nanocubes)/CdS composite photocatalysts: 0.25mg Pt nanocubic particles were added into 100mL water containing 0.05g commercial CdS photocatalyst. The commercial CdS was purchased from Shanghai Energy Chemical Company and used without further purification. The average particle diameter of the commercial CdS is 45.6nm and the surface area is 15.9 m^2/g. The resulting solution was stirred for 2h at room temperature. After centrifugation, the Pt/CdS composite was washed with high purity water and dried at 60°C under vacuum. UV-Vis absorption spectra indicate that there is no characterized absorption of Pt nanoparticles in the filtrate, indicating the Pt nanoparticles have been completely deposited onto the surface of CdS particles. The Pt loading is 0.5wt.% of CdS mass.

2.3 Photodeposition of Pt nanoparticles on CdS photocatalysts: Photodeposition of 0.5wt.% Pt on CdS was carried out using the method introduced previously.[23-25] In detail, 0.05g CdS was suspended in a 100ml 1.0M aqueous $(NH_4)_2SO_3$ solution. H_2PtCl_6 powder was added to the solution as a Pt source for the deposition of 0.5wt% of Pt cocatalyst on CdS particles. The solution was then thoroughly degassed and irradiated by a Xe lamp (Perfectlight Co., PLS-SXE300).

2.4 Characterizations: TEM/HRTEM images and selected area Energy Dispersive X-ray Spectroscopy (EDS) were obtained using a JEM-2100 transmission electron microscope (TEM) equipped with a Link EDS detector operated at 200KV. The X-ray diffraction (XRD) spectral measurements were conducted on a BRUKER-D8 X-ray diffractometer using Cu Ka radiation.

2.5 Electrochemical measurements: The electrochemical measurements were performed using a CHI 660E Electrochemical Analyzer in a standard three-electrode cell. A certain amount of Pt nanoparticles were dispersed in a water/ethanol (1:1) solution, and then an appropriate amount of 5.0 wt.% Nafion solution was added to the solution with a 1:5 volume ratio of Nafion solution to the water/ethanol solution. Working electrodes were prepared by dropping as-prepared Pt nanoparticle solution onto a glassy carbon electrode (GCE, 0.07cm^2) with the loading amount 100μg/cm^2. A saturated calomel electrode (SCE) and a large Pt foil were used as the reference electrode and the counter electrode, respectively. Cyclic voltammetry (CV) spectra were collected using two electrolytes: one was an aqueous solution containing 0.1M $HClO_4$ and 1.0M CH_3OH and the second was a 0.1M $HClO_4$ solution. The scan rates of CV spectral measurements were 50mV·s^{-1} for both electrolytes. But the potential range for the first electrolyte was from 0.00 to 0.65V (vs. SCE) and -0.15 to 0.75V (vs. SCE) for the second electrolyte. The electrochemically active surface area (EASA) was calculated based on the CV spectra of the 0.1M fresh $HClO_4$ solution.

2.6 Photocatalytic activity measurements: Visible light photocatalytic hydrogen production was carried out as follows: 0.05g prepared Pt/CdS powder was suspended in 100mL of 1.0M aqueous $(NH_4)_2SO_3$ solution. The solution was then transferred to a Pyrex glass reactor cell (Perfectlight Co., Labsolar-I). The system was vacuum-degassed and irradiated using a 300W Xe lamp (PLS-SXE300/300UV, Perfectlight Co.). A water filter was used to remove the infrared light portion of the Xe light spectrum and an optical cutoff filter was used to eliminate the UV radiation (< 420nm) (Supporting Information, Figure S1). The illumination intensity was 12.1mW/cm^2 from wavelength ranges of 410 to 520 nm. Hydrogen evolution was measured using an online gas chromatograph (Techcomp Limited Co., GC7890II) equipped with a thermal conductivity detector. The quantum efficiency (*Q.E.*) of the photocatalyst toward H_2 production is defined as: $Q.E. = 2*N_{H2}/N_P*100$. Where, N_{H2} and N_P refer to the number of generating hydrogen and the total number of incident photons arriving on the photocatalyst surface, respectively. An interference filter was used to ensure the incident light was centered at 420nm (Supporting Information, Figure S2). The illumination intensity was 0.59 mW cm^{-2} at 420nm.

3. Results and discussion

3.1 Preparation and Characterization of Pt nanoparticles (NPs) and Pt(NPs)/CdS: The reduction of $Pt(IV)Cl_6^{2-}$ ions in the presence of tetramethylammonium bromide yields an average particle size of 8.2 ±0.7nm Pt nanocubes and a shape selectivity of about 81% (Figure 1A). The shape selectivity in this research is defined as the number of cubic particles over the total number of nanoparticles synthesized. High-resolution TEM (HRTEM) images show that the Pt nanocubes are single crystals enclosed by six (100) crystal planes (Figure 1B). The distance between two Pt lattice fringes is 0.193nm, close to the distance of Pt {200} planes (0.196nm) in a face-centered cubic (fcc) Pt crystal. Selective area energy dispersive spectroscopy (EDS) and XRD patterns also agreed well with the standard Pt fcc data. The broadened XRD peaks of the sample indicate that the Pt cubes prepared are ultra-fine nanoparticles.

The shape and particle size of Pt nanocrystals can be controlled by the particle growth rate, depending on the reaction temperature and the molar ratio of $Pt(IV)Cl_6^{2-}$ to ($Pt(IV)Cl_6^{2-}$ + $Pt(II)Cl_4^{2-}$) in the initial solution.[21] TEM images indicate that Pt nanocubes with sizes of 6nm and 4nm were obtained when the molar ratio of $Pt(IV)Cl_6^{2-}/(Pt(IV)Cl_6^{2-} + Pt(II)Cl_4^{2-})$ was controlled at 0.8 and 0.2, respectively (Supporting Information, Figure S3). The shape selectivities of Pt nanocubes with an average particle size of 6nm (6.1 ± 1.0nm) and 4nm (4.2 ± 0.6nm) were measured to be ~ 85% and ~ 75%, respectively. HRTEM images revealed that the prepared Pt nanocubes, although of different sizes, are all enclosed by six (100) crystal planes (Inserts in Figure S3). In contrast, 4nm Pt nanospheres (with an average diameter of 4.0 ± 0.8nm) and 6nm Pt nanospheres (with an average diameter of 5.7 ± 0.5nm) were synthesized at 140°C when the $Pt(IV)Cl_6^{2-}/(Pt(IV)Cl_6^{2-} + Pt(II)Cl_4^{2-})$ ratio was maintained at 0.2 and 0.8, respectively.

The obtained Pt nanocube samples were subsequently dissolved in 100mL of pure water suspended with a certain amount of commercial CdS. The mixture was stirred at room temperature for 2h to allow the Pt nanoparticles to attach to the CdS surface. As shown in Figure S4 of the Supporting Information, the complete deposition of Pt nanoparticles onto CdS was confirmed by a UV-Vis adsorption method previously introduced.[23] Figure 2 shows a typical TEM image of the prepared semiconductor-metal nanocomposites with 0.5wt.% 4nm Pt nanocubes loaded (Pt(4nm NCs)/CdS). EDS performed on a single and darker particle confirms that the particle is a Pt particle. The observation shows that the shape and particle size of Pt nanoparticles on CdS do not change significantly before or after the photocatalytic reaction, suggesting that the prepared

Pt(NCs)/CdS is photochemically stable.

3.2 Photocatalytic activity of Pt(NCs)/CdS for hydrogen production: The photocatalytic activities of Pt(NCs)/CdS photocatalysts for visible light (λ > 420nm) photocatalytic hydrogen production were determined using an aqueous ammonium sulfite solution with a pH value close to 8.0. The baseline experiment shows that no hydrogen was generated in the dark under the experimental conditions. The photocatalytic activity of CdS was negligible. [23-25] In contrast, the prepared Pt(NCs)/CdS photocatalysts show much higher photocatalytic H_2 production activities (Figure 3). The rate of H_2 production over Pt(4nm NCs)/CdS photocatalyst is 1650μmol/h with a quantum efficiency of 56.3% under 420nm light irradiation. (Table S1 in Supporting Information) Experimental results also exhibit that the photocatalytic hydrogen production over prepared Pt(NCs)/CdS is stable. As shown in Figure 3, the rate of hydrogen evolution in the second experimental run is almost identical to that of the first experimental run. A total of 16.6mmol of H_2 was collected during 10 hours of reaction (Figure 3a). The turnover numbers defined as the molar ratio of the total hydrogen evolved to the photocatalyst CdS (0.346mmol) and to the Pt cocatalyst (1.28μmol) are about 48 and 12955, respectively. The very high turnover numbers indicate that hydrogen produced resulted from the photocatalytic oxidation of aqueous ammonium sulfite solution rather than from the photooxidation of Pt/CdS photocatalyst. The XRD of Pt/CdS also supports this conclusion because the XRD patterns of Pt/CdS photocatalyst remain unchanged before and after photocatalytic H_2 production. A Pt/CdS photocatalyst prepared by the photodeposition method was approved to be stable via a 64h lifespan test previously.[24] This result confirms that CdS photocorrosion can be avoided when an aqueous ammonium sulfite solution is used as a sacrificial material.

3.2.1 Effect of Pt particle shape on photocatalytic activity: Experimental results have indicated that the photocatalytic activity of Pt/CdS for H_2 production is heavily dependent on the shape of Pt particles. As shown in Figure 3b, the rate of H_2 production over Pt(4nm NCs)/CdS is nearly 31% higher than that over 4nm Pt irregular nanospheres loaded CdS (Pt(4nm NSPs)/CdS) photocatalyst under an identical condition and with the same Pt loading. Berr et al.[26] have pointed out that the hydrogen generation efficiency of Pt/CdS is a function of Pt coverage on the surface of CdS. Based on this result, the rates of H_2 production over Pt(4nm NCs)/CdS and Pt(4nm NSPs)/CdS are comparable to the same Pt nanoparticle coverage of the CdS photocatalyst. As shown in Table S1

and Figure S6 of Supporting Information, when the coverage of Pt nanoparticles is at 198 Pt particles/μm^2 of CdS the rate of hydrogen production over Pt(4nm NCs)/CdS (1650 μmol/h) is about 3.2 times higher than that of Pt(4nm NSPs)/CdS (515 μmol/h), This result indicates that the shape of Pt nanoparticles plays a key role in the photocatalytic activity of Pt/CdS photocatalysts. We notice that if the Pt particle coverage is a constant for Pt(4nm NCs)/CdS and Pt(4nm NSPs)/CdS, the Pt loading weight percentage does not remain the same. In this case, one may argue that the shape effect may result from the Pt loading percentage, but not from the shape of Pt nanoparticles. To further verify the shape effect, and rule out the interference of the Pt loading difference, we calculated the rate of hydrogen evolution in terms of per mg of Pt loading. The resulting hydrogen evolution rates for Pt(4nm NCs)/CdS and Pt (4nm NPs)/CdS were 6.6 mmol/h/mg of Pt and 4.6 mmol/h/mg of Pt, respectively. This significant difference further proves that Pt nanocube loaded CdS is 43.5% more effective in hydrogen production than is Pt nanosphere loaded CdS photocatalyst.

It should be pointed out that 4nm Pt nanocubes (with an average edge length of 4.2nm) reported in this paper have a much larger volume than that of 4nm Pt nanospheres (with an average diameter of 4.0nm). As shown in Table S2 (Supporting Information), the volume of one 4nm Pt cubic particle is 74nm^3. In contrast, the volume of a Pt nanosphere with its diameter of 4nm is only 33.5nm^3. If we compare the photocatalytic activities of Pt/CdS photocatalysts based on the similar volumes of Pt nanocubes and nanospheres, the result again strongly supports the shape effect of Pt nanocubes. For example, 6nm Pt nanospheres synthesized in this research have an average diameter of 5.7nm. The volume of this particle is 97nm^3, closer to 74nm^3 for 4nm Pt nanocubes than to 33.5nm^3 for 4nm Pt nanospheres. At the same Pt loading weight percentage the rate of hydrogen production for Pt(6nm NSPs)/CdS photocatalyst is 957μmol/h, compared to 1650μmol/h hydrogen evolution rate for Pt(4nm NCs)/CdS. We can conclude that a 72.4% rate increase has been achieved.

For further investigation of shape effect, Pt/CdS photocatalysts prepared via the facile two step method shown in this research are compared with a Pt/CdS prepared via conventional photodeposition method. The photocatalytic activity of Pt/CdS prepared by the photodeposition technology was measured under the same experimental conditions and Pt loading percentage as the shape controlled Pt/CdS photocatalysts. TEM imaging reveals that the photodeposited Pt metal

particles are irregular shaped nanospheres. This is due to the fact that the growth of the Pt particles is on the surface of CdS particles.[1-6, 14] The average particle size of the photoreduced Pt nanospheres over CdS is approximated as 2.6nm (Figure S5 of the Supporting Information). The rate of hydrogen production over Pt(4nm NCs)/CdS is 25% higher than that of photodeposited Pt/CdS photocatalysts. In this case, the shape effect is more pronounced because the average size of Pt nanoparticles via the photodeposited method is 35% smaller (2.6nm compared with 4.2nm) than 4nm Pt nanocubes, but the efficiency of Pt(4nm NCs)/CdS is 25% higher than Pt(2.6nm NSPs)/CdS. This result further confirms that the shape of Pt nanoparticles plays a vital role in Pt/CdS photocatalysts. Pt nanocubes loaded Pt(NCs)/CdS significantly enhances the hydrogen production rate in comparison with conventionally prepared Pt/CdS as well as shape controlled synthesis of Pt nanosphere loaded CdS photocatalysts.

3.2.2 Effect of Pt particle size on photocatalytic activity: Along with the shape effect of Pt particles, the particle size of Pt nanocubes also plays an important role in the hydrogen production of Pt/CdS photocatalyts. As shown in Figure 3b, for Pt nanocube loaded Pt(NCs)/CdS, the photocatalytic activity quickly decreases with the increase of particle size. The rate of H_2 production over Pt(8nm NCs)/CdS (900μmol/h) photocatalyst is about 50% of the rate for Pt(4nm NCs)/CdS photocatalyst. One likely reason for the enhanced photocatalytic activity of Pt(NCs)/CdS is the increased Pt work function when Pt particle size decreases. As reported in literature, the work function (Φ) of metal particles depends on their size[27] (*d*) and can be expressed as[28] $\Phi=\Phi_{\infty}(eV)+1.08(eV.nm)/d(nm)$, where d is the average size (nm) of the particles, Φ_{∞} is the work function of metal particles of infinitely large diameter. The higher work function for smaller Pt nanocubes indicates a higher Schottky barrier formed on the semiconductor-metal interface.[1, 2] This facilitates the rectification effect of the Pt-CdS junction and prolongs the lifespan of electrons remaining in Pt particles (Step 2 in water splitting/reducing process). In addition to the increase of work function, the smaller Pt particles have higher surface areas, leading to a higher H_2 generation rate.

3.3 Relationship between electrocatalytic activity of Pt particles and photocatalytic activity of Pt(NPs)/CdS: From an electrochemical viewpoint, the enhanced photocatalytic activity of Pt(NCs)/CdS compared to that of Pt(NSPs)/CdS can be attributed to the more effective proton reduction of Pt nanocubes (Step 3). Figure 4 shows the cyclic voltammograms (CVs) for Pt

nanocubes and nanospheres modified glassy carbon electrodes performed in a 0.1M $HClO_4$ electrolyte at a scan rate of $50mV \cdot s^{-1}$. The two peaks located at -0.097 and -0.032V (vs. SCE) in a positive sweep belong to hydrogen desorption on the surface of Pt particles. As shown in Figure 4 and Figure S7 of the Supporting Information, the activity order of electrocatalytic proton reduction of Pt NPs is as: 4nm Pt NCs > 6nm Pt NCs > 4nm Pt NSPs > 8nm Pt NCs. This sequence agrees well with the photocatalytic activities of Pt(NPs)/CdS composites.

The specific electrochemically active surface areas (EASAs) of 4nm, 6nm and 8nm Pt NCs and 4nm Pt NSPs modified electrodes were calculated from Figure 4 as 33.81, 29.72, 10.64 and 21.1m^2/g Pt, respectively. This calculation is based on EASA = $Q_H(C)/(0.210(mC/cm^2) \cdot L_{Pt}(g))$, where, $Q_H(C)$ is the area of hydrogen-adsorption/desorption peak measured by integrating CV curves from -0.2V to -0.74V (vs. SCE), L_{Pt} is the Pt particle loading (g) on the working electrode. The results show that the improved electrocatalytic activity of Pt(NCs) for proton reduction compared to that of Pt(NSPs) are attributed to the increased EASAs. The higher EASAs indicate an increased number of active sites of Pt particles for proton adsorption and desorption.[17] Furthermore, particular-shaped Pt nanoparticles, such as cubes, tetrahedrons and cuboctahedrons, have specific crystal planes exposed on the particle surfaces. Due to atom density differences, metal crystal planes show different electrocatalytic activities. Therefore, the atom density on the surface of Pt particles can be another possible explanation for the electrocatalytic activity differences of Pt nanocubes and Pt nanospheres [12].

Similar morphology and size dependent electrocatalytic properties for methanol electrochemical oxidation were observed using prepared Pt nanocrystals. The electrocatalytic activities of Pt NCs and Pt NSPs towards methanol electrochemical oxidation were determined in an aqueous solution containing 1.0M CH_3OH and 0.1M $HClO_4$. Pt nanocubes and Pt nanospheres modified glassy carbon electrodes were used as working electrodes (Figure S8 of the Supporting Information). The potentials of the CV measurements were converted to the potentials based on a saturated calomel electrode (SCE). As shown in Figure S8, the order of electrocatalytic activities of Pt NCs and Pt NSPs for methanol oxidation is: 4nm Pt NCs > 6nm Pt NCs > 4nm Pt NSPs > 8nm Pt NCs. This sequence is consistent with the decreasing order of EASAs for the Pt nanoparticles (Figure S9). The photocatalytic activities of Pt nanoparticle loaded Pt(NPs)/CdS photocatalysts also show sequence as those of electrocatalytic activities and EASAs of Pt NPs.

These results indicate for the first time that the photocatalytic activity of a Pt nanoparticle loaded CdS photocatalyst is strongly related to the electrocatalytic activities of shape- and size-controlled Pt nanoparticles. Cubic Pt nanoparticles have significantly higher EASAs and higher electrocatalytic activities and therefore higher photocatalytic activities for visible light photocatalytic hydrogen production.

3.4 Discussion of the shape effect of Pt NPs on the hydrogen production rate: Photocatalytic hydrogen evolution can be affected by multiple factors including cocatalyst shape, Pt particle sizes (or surface areas) and contact impedance (resistance and capacitance) between Pt particles and CdS surface. Under the same Pt loading, the shape and surface area of Pt nanoparticles play a major role. As shown in Figure 5, the photocatalytic hydrogen evolution rate is not linearly related to the total surface area of Pt nanoparticles, which is defined as individual particle surface area $*$ total number of Pt NPs. The calculation shows that total surface areas for both Pt cubic and spherical particles are $6M/\rho*a$, where M and ρ are Pt loading mass and density, respectively, and a is the Pt particle size. The detailed calculation can be found in the Supporting Information of this paper. The slopes of the curve (Figure 5) decline from 21.46μmol/h/cm^2 to 12.88μmol/h/cm^2 and finally to -4.28μmol/h/cm^2 for 8nm, 6nm and 4nm Pt nanocubes, respectively. The optimal Pt nanoparticle size corresponding to the maximum hydrogen production rate is at 4.4nm (160cm^2 total surface area) and with a 1682μmol/h hydrogen evolution rate. Further reducing particle size of Pt nanoparticles will lead to a decrease of hydrogen rate. The rate decline is attributed to two main factors: particle aggregation and blockage of light on the CdS surface (Pt nanoparticle coverage effect). When Pt nanoparticles become too small they tend to aggregate to reduce the surface energy. On the other hand, a higher Pt particle surface area blocks more light access to CdS, leading to a low hydrogen rate. Therefore further decreasing the size of Pt particles will not improve the hydrogen evolution rate. When reducing the size of Pt nanoparticles no longer enhances the hydrogen production rate, then the shape of Pt nanoparticles can control the photocatalytic activity of Pt/CdS photocatalysts.

When the edge sizes of Pt nanocubes equate to the diameter of Pt nanospheres, the two types of nanoparticles (cube and sphere) have the same total surface area (Supporting Information). As shown in Figure 5, the rate of hydrogen evolution increases from 1260μmol/h for Pt(4nm

NSPs)/CdS to 1650μmol/h for Pt(4nm NCs)/CdS, a 31% increase. However, the overall surface areas of these two Pt particles are the same. When Pt particle size is 5.7nm a 52% increase has been found, comparing Pt(5.7nm NCs)/CdS and Pt(5.7nm NSPs)/CdS. We can therefore conclude that the hydrogen rate improvement results from the shape effect of the Pt nanoparticles, and the shape impacts of Pt nanoparticles are dependent on their size. The shape effect is more significant for larger Pt particles than for smaller particles. It may be predicted that when Pt particle size reduces to a certain size the effect of Pt particle shape is minimized. Three major factors are responsible for the shape effect: (1) Spherical shaped Pt nanoparticles have a higher possibility for aggregation because their volumes are smaller than cubic particles when the average sizes for these two particles are the same. (Table S3, Supporting Information). (2) Pt nanocubes have higher atom density crystal planes for the proton adsorption and hydrogen formation than of that of Pt nanospheres. The vertexes and edges of the cubes have higher electrode densities and therefore promote electron transfer and increase the hydrogen formation rate. And finally, (3) Pt nanocubes have better contact with CdS crystals than Pt nanospheres, reducing the impedance between Pt/CdS conjunction and leading to the reduction of energy loss during the transportation of photo-induced electrons. A more detailed discussion would require more thorough modeling and computational assistance and is therefore beyond the scope of this paper.

4. Conclusion

Shape-and-size-controlled Pt nanocubes were prepared and loaded onto the surface of CdS photocatalysts (Pt(NCs)/CdS) for visible light photocatalytic hydrogen production via photocatalytic oxidation of aqueous ammonium sulfite solutions. The photocatalytic activity of Pt(NCs)/CdS photocatalysts strongly depends on both the shape and size of the Pt particles. The electrochemical characterization of Pt nanoparticles revealed that higher electrocatalytic activities of Pt nanoparticles correspond to higher efficiency of photocatalytic hydrogen evolution of Pt(NPs)/CdS. These results and observations confirm that the photocatalytic activity of a semiconductor-metal photocatalyst applied to water splitting/reducing is related to the electrocatalytic activity of the noble metals. The experimental result indicates that shape controlled synthesis of cocatalysts could be an innovative direction for the development of new and efficient semiconductor-metal photocatalysts for hydrogen production.

Supporting Information

The supporting information includes: (1) TEM images and size distributions of monolayer dispersed single-crystalline Pt nanoparticles; (2) Photodeposited Pt/CdS; (3) Comparison of photocatalytic hydrogen production at a same Pt nanoparticle coverage; (4) CV curves for prepared Pt nanocubes and nanospheres; and (5) Calculation of total surface areas of Pt nanoparticles.

Acknowledgment

This work was financially supported by the National Natural Science Foundation of China (21103106), Shanghai Key Project for Fundamental Research (13JC1402800), the ‘‘Dawn’’ Program of Shanghai Education Commission (11SG52) and Science and Technology Commission of Shanghai Municipality (14DZ2261000). We thank Professor Tetsuro Majima of Osaka University for his valuable comments.

References

1. X. Chen, S. Shen, L. Guo and S. S. Mao, *Chemical Reviews*, 2010, 110, 6503-6570.
2. A. L. Linsebigler, G. Lu and J. T. Yates, *Chemical Reviews*, 1995, 95, 735-758.
3. Z. Zou, J. Ye, K. Sayama and H. Arakawa, *Nature*, 2001, 414, 625-627.
4. K. Maeda, K. Teramura, D. Lu, T. Takata, N. Saito, Y. Inoue and K. Domen, *Nature*, 2006, 440, 295.
5. X. Wang, K. Maeda, A. Thomas, K. Takanabe, G. Xin, J. M. Carlsson, K. Domen and M. Antonietti, *Nature materials*, 2009, 8, 76-80.
6. J. Yang, D. Wang, H. Han and C. Li, *Accounts of chemical research*, 2013, 46, 1900-1909.
7. H. Chen, S. Chen, X. Quan, H. Yu, H. Zhao and Y. Zhang, *The Journal of Physical Chemistry C*, 2008, 112, 9285-9290.
8. V. Subramanian, E. E. Wolf and P. V. Kamat, *Journal of the American Chemical Society*, 2004, 126, 4943-4950.
9. J. J. Burton, *Catalysis Reviews*, 1974, 9, 209-222.
10. J. Zhang, C. Feng, Y. Deng, L. Liu, Y. Wu, B. Shen, C. Zhong and W. Hu, *Chemistry of Materials*, 2014, 26, 1213-1218.
11. A. X. Yin, X. Q. Min, Y. W. Zhang and C. H. Yan, *Journal of the American Chemical Society*, 2011, 133, 3816-3819.
12. R. Narayanan and M. A. El-Sayed, *Nano Letters*, 2004, 4, 1343-1348.
13. S. Rawalekar and T. Mokari, *Advanced Energy Materials*, 2013, 3, 12-27.
14. R. Asahi, T. Morikawa, T. Ohwaki, K. Aoki and Y. Taga, *Science*, 2001, 293, 269-271.
15. M. Berr, A. Vaneski, A. S. Susha, J. Rodriguez-Fernandez, M. Doeblinger, F. Jaeckel, A. L. Rogach and J. Feldmann, *Applied Physics Letters*, 2010, 97.
16. A. Vaneski, A. S. Susha, J. Rodriguez-Fernandez, M. Berr, F. Jaeckel, J. Feldmann and A. L. Rogach, *Advanced Functional Materials*, 2011, 21, 1547-1556.
17. M. J. Berr, A. Vaneski, C. Mauser, S. Fischbach, A. S. Susha, A. L. Rogach, F. Jaeckel and J. Feldmann, *Small*, 2012, 8, 291-297.
18. M. J. Berr, P. Wagner, S. Fischbach, A. Vaneski, J. Schneider, A. S. Susha, A. L. Rogach, F. Jaeckel and J. Feldmann, *Applied Physics Letters*, 2012, 100.
19. F. F. Schweinberger, M. J. Berr, M. Doeblinger, C. Wolff, K. E. Sanwald, A. S. Crampton, C. J. Ridge, F. Jaeckel, J. Feldmann, M. Tschurl and U. Heiz, *Journal of the American Chemical Society*, 2013, 135, 13262-13265.
20. Y. Negishi, M. Mizuno, M. Hirayama, M. Omatoi, T. Takayama, A. Iwase and A. Kudo, *Nanoscale*, 2013, 5, 7188-7192.
21. C. K. Tsung, J. N. Kuhn, W. Huang, C. Aliaga, L. I. Hung, G. A. Somorjai and P. Yang, *Journal of the American Chemical Society*, 2009, 131, 5816-5822.
22. M. Luo, Y. Hong, W. Yao, C. Huang, Q. Xu and Q. Wu, *J. Mater. Chem. A*, 2014, DOI: 10.1039/c4ta05250a.
23. W. Yao, C. Huang, N. Muradov and A. T-Raissi, *International Journal of Hydrogen Energy*, 2011, 36, 4710-4715.
24. J. Zhang, W. Yao, M. Liu, Q. Xu, Q. Wu and T. Zeng, *Catalysis Letters*, 2013, 143, 1030-1034.
25. B. Zhang, W. Yao, C. Huang, Q. Xu and Q. Wu, *International Journal of Hydrogen Energy*, 2013, 38, 7224-7231.

26. M. J. Berr, F. F. Schweinberger, M. Doblinger, K. E. Sanwald, C. Wolff, J. Breimeier, A. S. Crampton, C. J. Ridge, M. Tschurl, U. Heiz, F. Jackel and J. Feldmann, *Nano letters*, 2012, 12, 5903-5906.
27. D. Wood, *Physical Review Letters*, 1981, 46, 749-749.
28. Y. Shiraishi, H. Sakamoto, Y. Sugano, S. Ichikawa and T. Hirai, *ACS nano*, 2013, 7, 9287-9297.

Figure Legends

Scheme 1. Schematic diagrams of (A) photocatalytic and (B) electrocatalytic hydrogen production.

Figure 1. (A) TEM and HRTEM images, (B) Nanoparticle size distribution, (C) Selected area energy dispersive spectroscopy and (D) XRD patterns of prepared 8nm single-crystalline Pt nanocubes.

Figure 2. TEM images of 4nm Pt(NCs)/CdS before (A) and after (B) visible light photocatalytic hydrogen production and (C) selected area energy dispersive spectroscopy (EDS) for a single Pt particle.

Figure 3. (A) Hydrogen evolution on 4nm Pt(NCs)/CdS and (B) rates of hydrogen production over different shapes and sizes of Pt nanoparticle loaded Pt/CdS photocatalysts.

Figure 4. CV curves of the prepared Pt nanocubes and nanospheres in 0.1M $HClO_4$ solution at a scan rate of 50 $mV \cdot s^{-1}$.

Figure 5 Photocatalytic hydrogen evolution rate as a function of total Pt nanoparticle surface area.

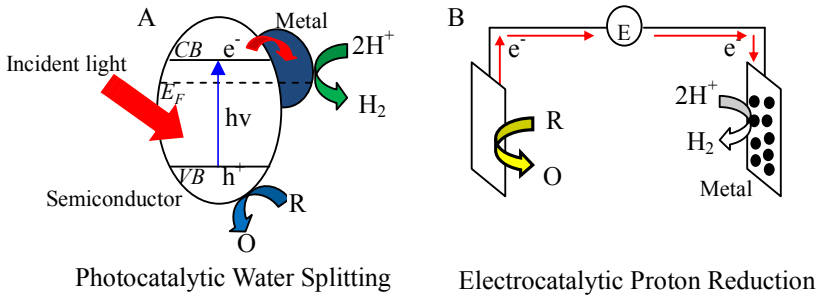

Scheme 1. Schematic diagrams of (A) photocatalytic and (B) electrocatalytic hydrogen production.

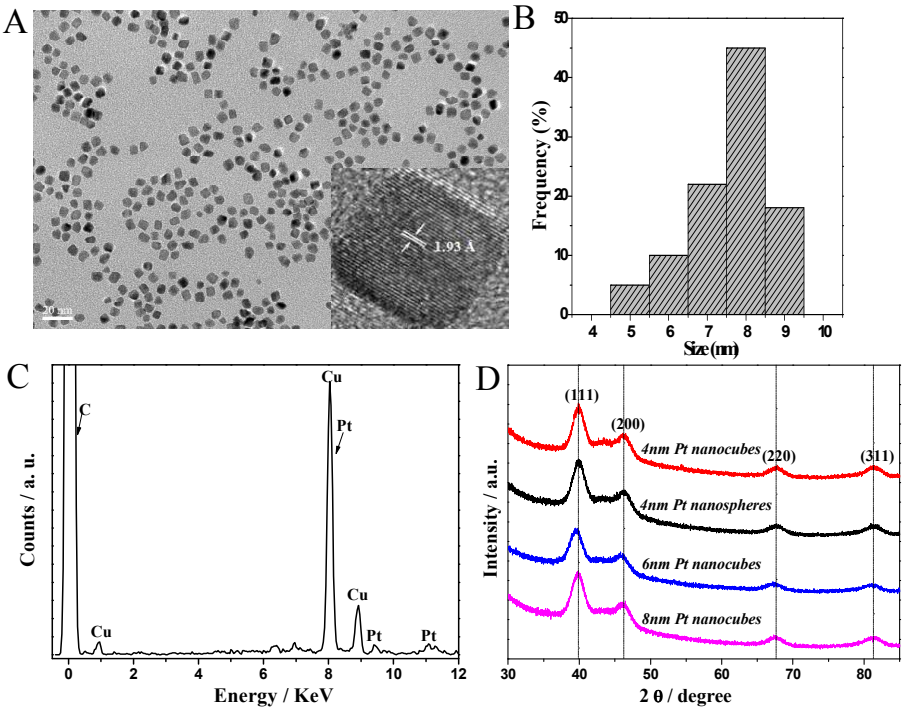

Figure 1. (A) TEM and HRTEM images, (B) Nanoparticle size distribution, (C) Selected area energy dispersive spectroscopy and(D) XRD patterns of prepared 8nm single-crystalline Pt nanocubes.

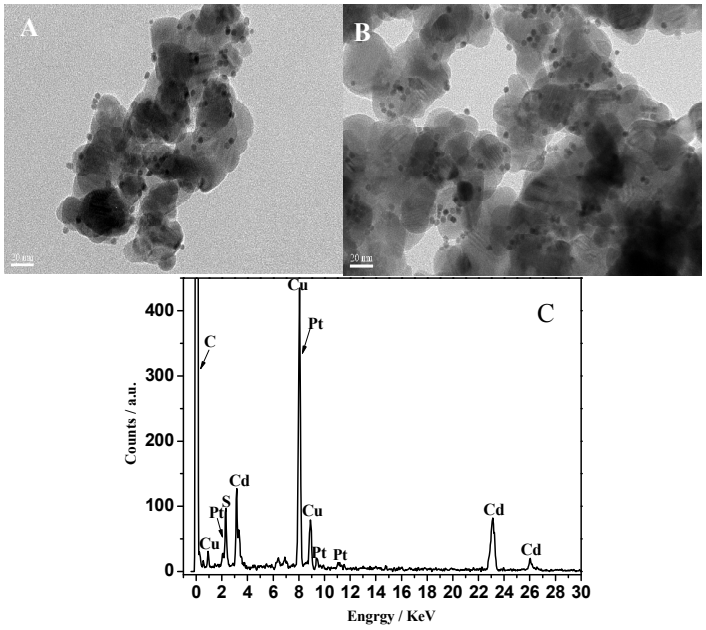

Figure 2. TEM images of 4nm Pt(NCs)/CdS before (A) and after (B) visible light photocatalytic hydrogen production and (C) selected area energy dispersive spectroscopy (EDS) for a single Pt particle.

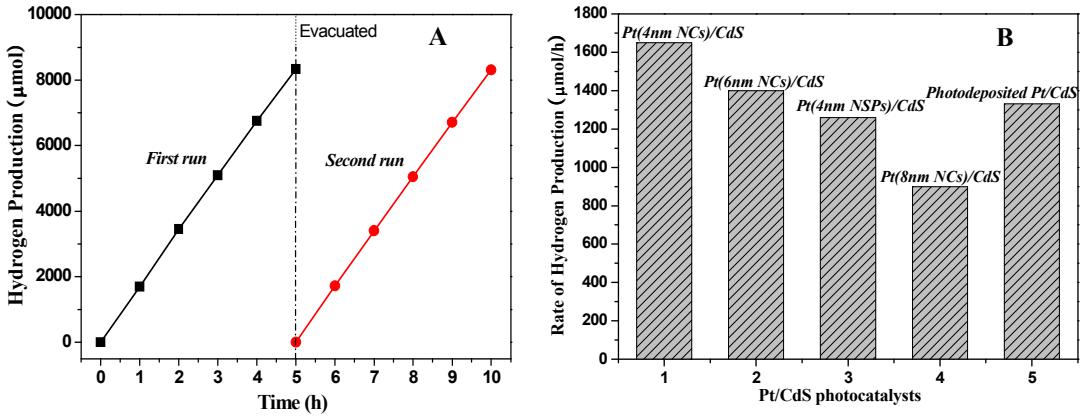

Figure 3. (A) Hydrogen evolution on Pt(4nm NCs)/CdS and (B) rates of hydrogen production over different shapes and sizes of Pt nanoparticle loaded Pt/CdS photocatalysts.

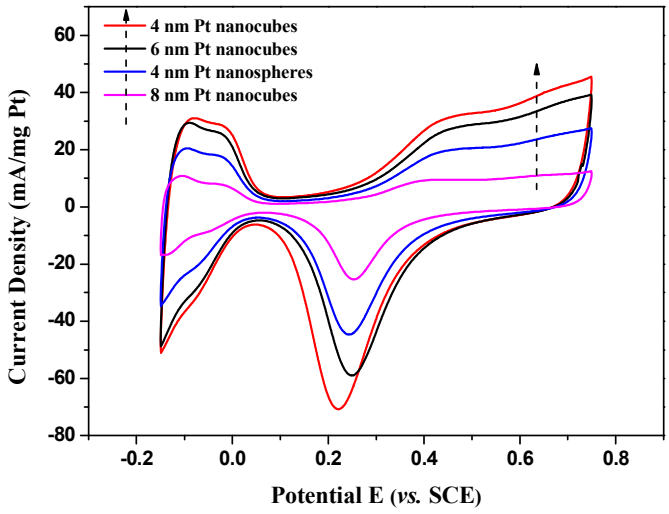

Figure 4. CV curves of the prepared Pt nanocubes and nanospheres in 0.1M $HClO_4$ solution at a scan rate of 50 $mV \cdot s^{-1}$.

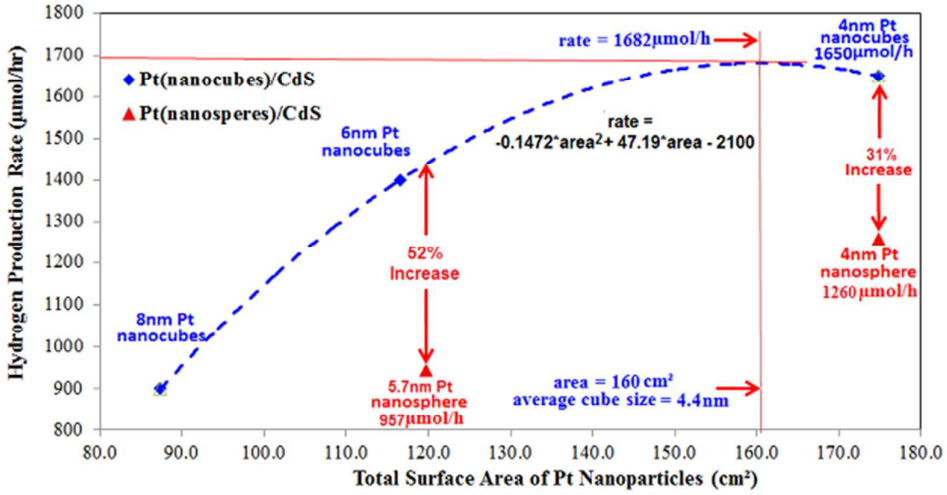

Figure 5. Photocatalytic hydrogen evolution rate as a function of total Pt nanoparticle surface area

Table of Content

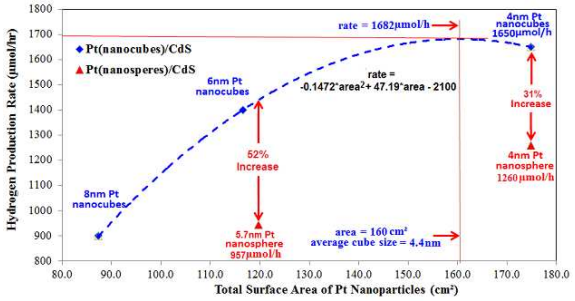

The photocatalytic activity of Pt/CdS photocatalysts strongly depends on both the shape and size of the Pt particles.